Melting of charge density wave and Mott gap collapse on $1T$-TaS_2 induced by interfacial water

Shiwei Shen,[1] Xiaoqiu Yuan,[1] Chenhaoping Wen,[1] Jingjing Gao,[2,3] Xuan Luo,[2] Xinghua Lu,[4] Yu-Ping Sun,[2,5,6] and Shichao Yan[1,7,*]

[1]*School of Physical Science and Technology, ShanghaiTech University, Shanghai 201210, China*
[2]*Key Laboratory of Materials Physics, Institute of Solid State Physics, Chinese Academy of Sciences, Hefei 230031, China*
[3]*University of Science and Technology of China, Hefei 230026, China*
[4]*Beijing National Laboratory for Condensed-Matter Physics and Institute of Physics, Chinese Academy of Sciences, Beijing, 100190, China*
[5]*High Magnetic Field Laboratory, Chinese Academy of Sciences, Hefei 230031, China*
[6]*Collaborative Innovation Centre of Advanced Microstructures, Nanjing University, Nanjing 210093, China*
[7]*ShanghaiTech Laboratory for Topological Physics, ShanghaiTech University, Shanghai 201210, China*

(Received 8 April 2020; accepted 3 June 2020; published 22 June 2020)

Microscopically revealing the interactions between interfacial water and the quantum states of matter is an important task from both the materials science and the physics points of view. Here we report a low-temperature scanning tunneling microscopy (STM) and spectroscopy study of water adsorption on the charge density wave compound $1T$-TaS_2, which has a Mott-insulating ground state. Interfacial water forms monolayer islands with 6×6 superstructures on the surface of $1T$-TaS_2, and the charge order under water islands can be directly imaged in STM topographies taken with negative bias voltages. Compared with the original $\sqrt{13} \times \sqrt{13}$ charge order in $1T$-TaS_2, the charge order under water islands becomes significantly disordered and denser. A V-shaped gaplike feature emerges in water-covered $1T$-TaS_2, which may be due to the enhanced dielectric constant of interfacial water, which reduces short-range Coulomb repulsion and induces Mott gap collapse. Our observations open the way to microscopically understanding the interactions between interfacial water and the correlated quantum states of matter.

DOI: 10.1103/PhysRevMaterials.4.064007

Interfacial water not only plays an important role in many fundamental phenomena such as heterogeneous catalysis, electrochemistry, and corrosion [1,2], but also has significant influence on the properties of solid materials. For example, it has been found that interfacial water modulates the electronic properties of two-dimensional materials [3]. More interestingly, the superconducting transition temperatures (T_c) of many unconventional superconductors strongly depend on the interactions with interfacial water: (i) the T_c of cuprate superconductors can be significantly degraded by interaction with water [4]; (ii) water can enhance the T_c of iron-based superconductors [5]; and (iii) water plays a critical role in the superconducting properties of hydrated materials, such as $Na_xCoO_2 \cdot yH_2O$ [6]. However, the precise roles of interfacial water in the superconducting and correlated electronic states of materials remain mysterious.

The scanning probe microscope (SPM) has proved to be an important tool for studying interfacial/surface water and can reach a submolecular resolution [2,7–11]. However, because most SPM studies focus on characterizing the atomic structures and the dynamic behaviors of water clusters on surfaces [2,8,9,12,13], it has not been possible so far to microscopically reveal the influences of interfacial water on the correlated quantum states of matter.

Here we use low-temperature scanning tunneling microscopy (STM) and spectroscopy (STS) to study the influences of interfacial water on the electronic states of a charge density wave (CDW) compound with a Mott-insulating ground state, $1T$-TaS_2 [Fig. 1(a)]. $1T$-TaS_2 has attracted great interest because of its rich electronic phases such as the CDW [14–16], the Mott-insulating state [17–19], superconductivity [20], and quantum spin-liquid behaviors [21]. Below 180 K, $1T$-TaS_2 enters a commensurate charge density wave (C-CDW) state with a $\sqrt{13} \times \sqrt{13}$ superlattice [Fig. 1(b)], where the displacement of the atoms leads to the formation of "Star of David" clusters [inset in Fig. 1(b)] [15]. The C-CDW state can either be viewed as a triple CDW, or in terms of a polaron picture, it can be treated as hexagonally packed localized polarons which are formed by a central Ta atom surrounded by 12 Ta atoms displaced toward it [15,22].

High-quality single crystals of $1T$-TaS_2 were grown by the chemical vapor transport method. STM experiments were carried out with a Unisoku low-temperature scanning tunneling microscope at the base temperature of 4.5 K. $1T$-TaS_2 single-crystal samples were cleaved *in situ* under ultrahigh vacuum and transferred into the STM head for precooling. The precooled $1T$-TaS_2 sample was then moved to the water dosing stage. Water was purified by a few freeze-pump-thaw cycles before being introduced into the vacuum chamber via a variable leak valve. During water dosing, the $1T$-TaS_2 sample was warmed up to $\sim$100 K. After water dosing, the

*yanshch@shanghaitech.edu.cn

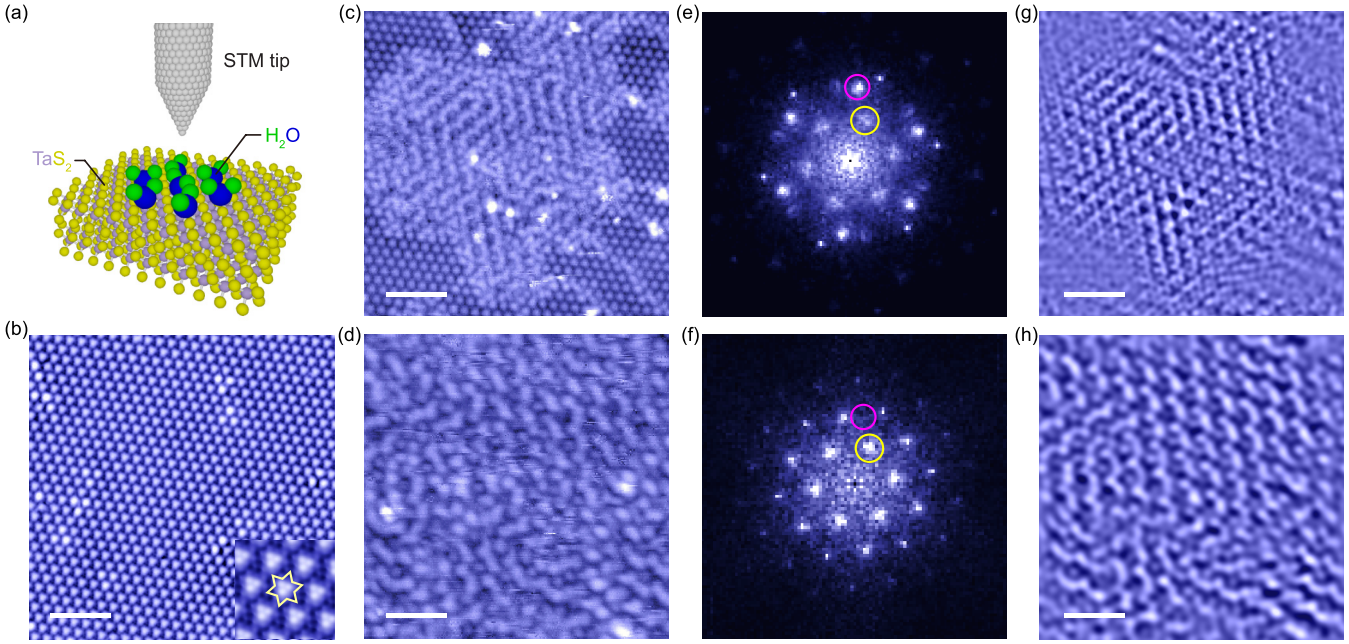

FIG. 1. (a) Schematic showing the measurements: STM tip and water islands on top of the $1T$-TaS_2 surface. (b) Constant-current STM topography on pristine $1T$-TaS_2 showing the $\sqrt{13} \times \sqrt{13}$ C-CDW superlattice ($V_s = 500$ mV, $I = 200$ pA). Inset: Zoom-in view of the C-CDW order; the "Star of David" structure is shown in light yellow. Scale bar: 6 nm. (c) Constant-current STM topography on water-covered $1T$-TaS_2 with a positive STM bias voltage ($V_s = 500$ mV, $I = 5$ pA). Scale bar: 6 nm. (d) Constant-current STM topography taken on water islands with a positive STM bias voltage ($V_s = 500$ mV, $I = 5$ pA). Scale bar: 4 nm. (e, f) FT of (c) and (d). Purple circles indicate $\sqrt{13} \times \sqrt{13}$ CDW peaks, and yellow circles indicate 6×6 wave vectors. (g, h) Inverse Fourier transform by selecting the 6×6 wave vectors and their second-order wave vectors in (e) and (f), respectively.

$1T$-TaS_2 sample was immediately transferred into the STM head for measurements. STS measurements were done by using standard lock-in technique with 5-mV modulation at the frequency of 914 Hz.

Figure 1(c) shows monolayer water islands on the $1T$-TaS_2 surface. As can be seen, water forms superstructures on the $1T$-TaS_2. In order to show the periodicity of the water superstructures, we performed Fourier transform (FT) on constant-current STM topographies. Figure 1(e) shows the FT of STM topography containing both water islands and bare $1T$-TaS_2 surface [Fig. 1(c)], and Fig. 1(f) shows the FT of STM topography taken on water islands [Fig. 1(d)]. Comparing these two FT images [Figs. 1(e) and 1(f)], we can see that the wave vector shown in the purple circle disappears in Fig. 1(f), which indicates that this is the $\sqrt{13} \times \sqrt{13}$ charge order vector of $1T$-TaS_2. Taking the $\sqrt{13} \times \sqrt{13}$ charge order as a reference, we can also identify the wave vectors shown in the yellow circles in Figs. 1(e) and 1(f) as 6×6 wave vectors. In order to clearly show the 6×6 superstructures, we performed selected inverse Fourier transform of 6×6 wave vectors and their second-order wave vectors [Figs. 1(g) and 1(h)], where the 6×6 superstructures can be clearly seen in water islands.

One interesting feature about the water islands is that they appear differently in STM topographies taken with positive and negative bias voltages. In STM topography with a positive bias voltage [Fig. 2(a)], monolayer water islands on $1T$-TaS_2 are $\sim$50 pm higher than the bare $1T$-TaS_2 region [Fig. 2(d)]. In STM topography with a negative bias voltage [Fig. 2(b)], the water-covered $1T$-TaS_2 region has almost the same height as the bare $1T$-TaS_2 region [Fig. 2(d)]. This indicates that water makes little contribution to the density of states between the Fermi level and the negative bias voltage used for imaging. This makes water islands "transparent" in negative-bias-voltage STM topography where the charge order of $1T$-TaS_2 under water islands can be directly imaged [Fig. 2(b)]. Surprisingly, compared with the well-ordered $\sqrt{13} \times \sqrt{13}$ charge order in pristine $1T$-TaS_2, the charge order in water-covered $1T$-TaS_2 regions is significantly disordered and denser [Fig. 2(b)]. This interfacial-water-induced disordered charge order is different from the thermally induced CDW transition to a nearly commensurate CDW state (above 180 K), where there are localized $\sqrt{13} \times \sqrt{13}$ charge order regions that are separated by CDW domain walls [23,24].

In order to characterize the periodicity of the charge order under water islands, we performed FT on constant-current STM topographies taken with negative bias voltages. In the FT image of STM topography with both water-covered and bare $1T$-TaS_2 surfaces [Figs. 2(b) and 2(c)], in addition to the $\sqrt{13} \times \sqrt{13}$ charge order, there are two additional wave vectors near each $\sqrt{13} \times \sqrt{13}$ charge order: one corresponds to the 3×3 charge order (in the orange circle), and the other is the $2\sqrt{3} \times 2\sqrt{3}$ charge order (in the green circle). In the FT of STM topography containing only water-covered $1T$-TaS_2 regions [Figs. 2(e) and 2(g)], the $\sqrt{13} \times \sqrt{13}$ charge order peak completely disappears, and the 3×3 and $2\sqrt{3} \times 2\sqrt{3}$ wave vectors remain. This demonstrates that the charge order in the water-covered $1T$-TaS_2 region is neither a charge order with single periodicity nor completely disordered. It is rather a

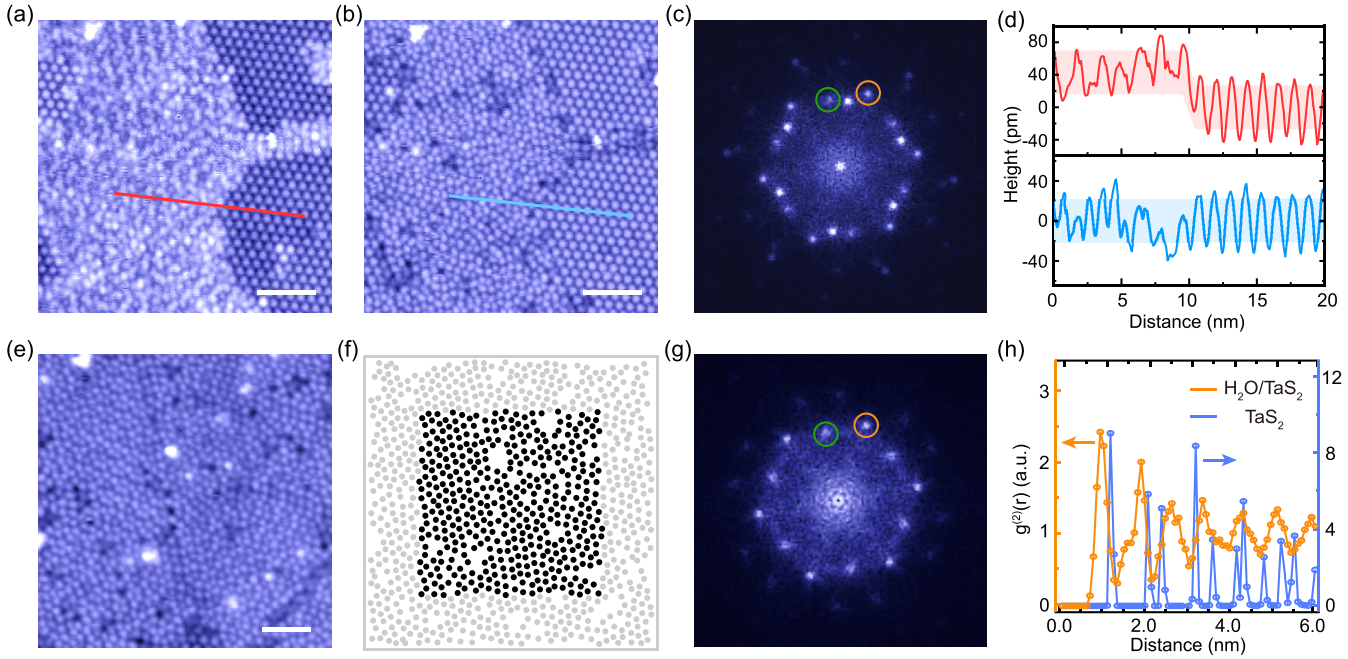

FIG. 2. (a) Constant-current STM topography on water-covered $1T$-TaS_2 with a positive STM bias voltage ($V_s = 500$ mV, $I = 5$ pA). (b) Constant-current STM topography taken on the same region as (a) with a negative STM bias voltage ($V_s = -500$ mV, $I = 5$ pA). Scale bar for (a) and (b): 6.4 nm. (c) FT of (b). (d) Line-cut profiles taken along the red (upper) and blue (lower) lines in (a) and (b). (e) Constant-current STM topography containing only a water-covered $1T$-TaS_2 region ($V_s = -500$ mV, $I = 5$ pA). Scale bar: 5 nm. (f) A polaronic pattern extracted from (e). Black dots indicate the point positions which are used in the calculation of polaronic pair distribution functions (PDFs) in (h). (g) FT of (e). Orange and green circles indicate 3×3 and $2\sqrt{3} \times 2\sqrt{3}$ wave vectors, respectively. (h) Polaronic PDFs, $g^{(2)}(r)$, for polaronic patterns in STM images taken on a water-covered $1T$-TaS_2 region (orange) and a pristine $1T$-TaS_2 surface (blue).

mixed charge order consisting of two sets of hexagonal wave vectors, which makes the charge order appear disordered in STM topography [Fig. 2(e)].

Another clear feature shown in Fig. 2(b) is that the pattern in the water-covered $1T$-TaS_2 region is denser than that in the bare $1T$-TaS_2 region. In terms of the polaron picture, STM topography on the water-covered region [Fig. 2(e)] can be taken as a lattice of localized polarons where each bulb can be treated as one localized polaron [22]. In order to show the average nearest-neighbor distance between two localized polarons, we first extract the positions of each polaron in same-sized areas of pristine and water-covered $1T$-TaS_2 [Figs. 2(f) and S2] [25], then calculate the polaronic pair distribution functions (PDFs), $g^{(2)}(r)$, which describe the probability of finding a particle at distance r from a given particle [22]. As shown in Fig. 2(h), the nearest-neighbor distances for localized polarons in the disordered charge order state and C-CDW state of $1T$-TaS_2 are $\sim$1.0 nm and $\sim$1.2 nm, respectively. This clearly indicates that the polaron density under water islands is about 1.2 times that in the C-CDW state of $1T$-TaS_2. There are only two pronounced peaks in the polaronic PDFs of $1T$-TaS_2 under water islands [Fig. 2(h)], which implies a lack of long-range correlations at $r > 3$ nm. We note that although the polaronic PDFs showing in $1T$-TaS_2 under water islands are quite similar to the polaronic PDFs in the recently reported amorphous metastable state induced by ultrafast laser pulses on $1T$-TaS_2 [22,25], instead of being in an amorphous state, there are clearly two sets of wave vectors for the lattice of polarons in water-covered $1T$-TaS_2 [Fig. 2(g)].

As shown in Figs. 3(a) and 3(b), the structure of water islands changes during the taking of STM images, which could be due to the perturbation of the STM tip or due to the quantum tunneling of protons in hydrogen-bonded water molecules. The structural changes in water islands also induce changes in the polaron pattern under water islands [Figs. 3(c) and 3(d)]. This indicates that polarons can be locally created or eliminated by water molecules [as shown in the green circles in Figs. 3(c) and 3(d)]. Based on this effect, the formation of disordered polaron patterns under water islands can be explained by the theoretical model developed by Vodeb *et al.* [26,27]. The hydrogen-bonded water dipoles screen and melt the charge order of $1T$-TaS_2 [28], which induces a larger number of polarons to form than in the C-CDW state of $1T$-TaS_2. These polarons prefer to form a hexagonal lattice due to the repulsion between them. At the polaron density under water islands, regular hexagonal polaron lattices cannot form because they are not commensurate with the underlying atomic lattice of $1T$-TaS_2, which results in a disordered polaron pattern in water-covered $1T$-TaS_2 [26,27].

After analyzing the structures of the interfacial-water-induced disordered polaron pattern, we performed STS to study how interfacial water affects the electronic states of $1T$-TaS_2. At low temperatures, the ground state of $1T$-TaS_2 is a Mott-insulating state with a lower Hubbard band and an upper Hubbard band at energies of about ± 200 meV [the

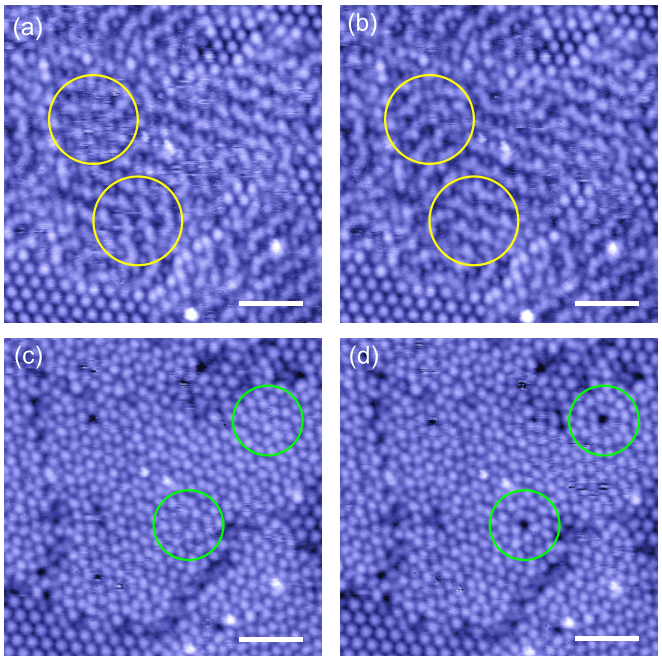

FIG. 3. (a–d) Sequence of STM images showing the changes in water clusters (a, b) and the changes in the disordered polaron pattern (c, d). Setup conditions: $V_s = 500$ mV, $I = 5$ pA for (a) and (b); $V_s = -500$ mV, $I = 5$ pA for (c) and (d). Yellow and green circles indicate the most significant changes in STM images taken with positive and negative bias voltages, respectively. Scale bar: 5 nm.

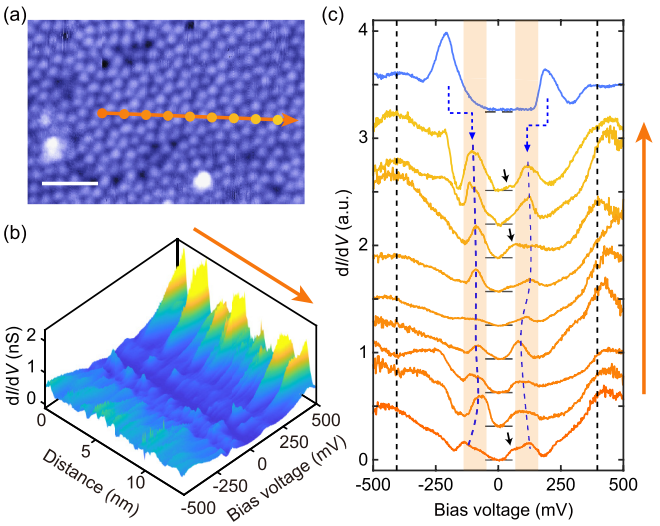

FIG. 4. (a) Constant-current STM topography on water-covered $1T$-TaS_2 with a negative STM bias voltage ($V_s = -500$ mV, $I = 5$ pA). Scale bar: 4 nm. (b) Three-dimensional plot of dI/dV line cut along the orange arrow shown in (a). (c) dI/dV spectra (orange and yellow) obtained at equally spaced positions along the line shown in (a), and a typical dI/dV spectrum taken on a pristine $1T$-TaS_2 surface (blue). Dashed blue lines show the evolution of the Hubbard bands. Dashed black lines indicate the positions of the conduction and valence bands. Short horizontal lines indicate $dI/dV = 0$ for each spectrum. Short black arrows indicate the emerged in-gap states near the Fermi level.

blue curve in Fig. 4(c)] [19]. As shown by the dashed vertical lines in Fig. 4(c), there are another two broad peaks, at about -400 mV and $+360$ mV, which correspond to the valence-band (VB) peak and conduction-band (CB) peak of $1T$-TaS_2, respectively [29,30]. Figure 4(b) is a three-dimensional plot of line-cut dI/dV spectra on water-covered $1T$-TaS_2 [Fig. 4(a)], and the yellow and orange spectra in Fig. 4(c) are the dI/dV spectra taken on the dots in Fig. 4(a). As shown, although the dI/dV spectra on water-covered $1T$-TaS_2 are inhomogeneous, there are clearly four common features compared with pristine $1T$-TaS_2 [25]: (i) the positions of the VB and CB remain almost unchanged, and the CB has a larger spectral weight than in pristine $1T$-TaS_2; (ii) the lower Hubbard band and upper Hubbard band peaks move closer to the Fermi level, and the Mott gap in water-covered $1T$-TaS_2 is about two times smaller than in pristine $1T$-TaS_2; (iii) a V-shaped gaplike feature emerges near the Fermi level, and the minimum of the V-shaped feature is pinned at the Fermi level; and (iv) as shown by the black arrows in Fig. 4(c), in-gap states emerge in some water-covered $1T$-TaS_2 regions.

On water islands, the intensity of the CB is significantly more enhanced than the VB, and the additional density of states near the CB may be contributed by water molecules. Mott gap collapse in water-covered $1T$-TaS_2 can generally be explained by the reduced ratio between the Coulomb repulsion U and the bandwidth W (U/W) within one band Hubbard model [17,18,30]. As shown in the dI/dV spectra in water-covered $1T$-TaS_2 [Figs. 4(b) and 4(c)], the bandwidths of the lower Hubbard band and upper Hubbard band show no significant change. This indicates that the decrease in U is likely the dominant factor for the Mott gap collapse in water-covered $1T$-TaS_2. Compared with pristine $1T$-TaS_2, water-covered $1T$-TaS_2 is covered by water islands which have an enhanced dielectric constant [28]. This enhanced dielectric constant of water reduces U in water-covered $1T$-TaS_2, which agrees with recent theoretical predications about Coulomb engineering of a Mott insulator by controlling its dielectric environment [31].

In summary, our observations clearly show that interfacial water forms superstructures on the $1T$-TaS_2 surface and induces the melting of CDW and Mott gap collapse on $1T$-TaS_2. We believe our work will be helpful for understanding the precise roles of interfacial water in other correlated electron materials [4–6] and stimulate further theoretical investigations about the interactions between interfacial water and quantum states of matter. Furthermore, we also demonstrate that due to the enhanced dielectric constant, interfacial water may provide a new way of controlling the Mott-insulating state of materials by Coulomb engineering.

The authors thank Vidya Madhavan, Atsushi Fujimori, Sheng Meng, Bin Shao, Zhenyu Wang, and Zhengwei Nie for fruitful discussions. S.Y. acknowledges financial support from the Science and Technology Commission of Shanghai Municipality (STCSM) (Grant No. 18QA1403100) and National Science Foundation of China (Grant No. 11874042) and startup funding from ShanghaiTech University. J.J.G., X.L., and Y.P.S. appreciate the support of the

National Key Research and Development Program under Contract No. 2016YFA0300404, the National Nature Science Foundation of China under Contracts No. 11674326 and No. 11874357, and the Joint Funds of the National Natural Science Foundation of China and the Chinese Academy of Sciences' Large-Scale Scientific Facility under Contracts No. U1832141 and No. U1932217.

S.S. and X.Y. contributed equally to this work.

[1] M. A. Henderson, Surf. Sci. Rep. **46**, 1 (2002).
[2] J. Carrasco, A. Hodgson, and A. Michaelides, Nat. Mater. **11**, 667 (2012).
[3] C. Melios, C. E. Giusca, V. Panchal, and O. Kazakova, 2D Mater. **5**, 022001 (2018).
[4] S.-G. Jin, Z.-Z. Zhu, L.-M. Liu, and Y.-L. Huang, Solid State Commun. **74**, 1087 (1990).
[5] H. Hiramatsu, T. Katase, T. Kamiya, M. Hirano, and H. Hosono, Phys. Rev. B **80**, 052501 (2009).
[6] K. Takada, H. Sakurai, E. Takayama-Muromachi, F. Izumi, R. A. Dilanian, and T. Sasaki, Nature **422**, 53 (2003).
[7] H.-J. Shin, J. Jung, K. Motobayashi, S. Yanagisawa, Y. Morikawa, Y. Kim, and M. Kawai, Nat. Mater. **9**, 442 (2010).
[8] J. Guo, X. Meng, J. Chen, J. Peng, J. Sheng, X.-Z. Li, L. Xu, J.-R. Shi, E. Wang, and Y. Jiang, Nat. Mater. **13**, 184 (2014).
[9] D. Halwidl, B. Stöger, W. Mayr-Schmölzer, J. Pavelec, D. Fobes, J. Peng, Z. Mao, G. S. Parkinson, M. Schmid, F. Mittendorfer, J. Redinger, and U. Diebold, Nat. Mater. **15**, 450 (2016).
[10] R. Ma, D. Cao, C. Zhu, Y. Tian, J. Peng, J. Guo, J. Chen, X.-Z. Li, J. S. Francisco, X. C. Zeng, L.-M. Xu, E.-G. Wang, and Y. Jiang, Nature **577**, 60 (2020).
[11] L. R. Merte, R. Bechstein, G. Peng, F. Rieboldt, C. A. Farberow, H. Zeuthen, J. Knudsen, E. Lægsgaard, S. Wendt, M. Mavrikakis, and F. Besenbacher, Nat. Commun. **5**, 4193 (2014).
[12] A. Michaelides and K. Morgenstern, Nat. Mater. **6**, 597 (2007).
[13] A. Dong, L. Yan, L. Sun, S. Yan, X. Shan, Y. Guo, S. Meng, and X. Lu, ACS Nano **12**, 6452 (2018).
[14] J. Wilson, F. D. Salvo, and S. Mahajan, Adv. Phys. **24**, 117 (1975).
[15] R. E. Thomson, B. Burk, A. Zettl, and J. Clarke, Phys. Rev. B **49**, 16899 (1994).
[16] K. Rossnagel, J. Phys.: Condens. Matter **23**, 213001 (2011).
[17] L. Ma, C. Ye, Y. Yu, X. F. Lu, X. Niu, S. Kim, D. Feng, D. Tománek, Y.-W. Son, X. H. Chen, and Y. Zhang, Nat. Commun. **7**, 10956 (2016).
[18] D. Cho, S. Cheon, K.-S. Kim, S.-H. Lee, Y.-H. Cho, S.-W. Cheong, and H. W. Yeom, Nat. Commun. **7**, 10453 (2016).
[19] J.-J. Kim, W. Yamaguchi, T. Hasegawa, and K. Kitazawa, Phys. Rev. Lett. **73**, 2103 (1994).
[20] B. Sipos, A. F. Kusmartseva, A. Akrap, H. Berger, L. Forró, and E. Tutis, Nat. Mater. **7**, 960 (2008).
[21] K. T. Law and P. A. Lee, Proc. Natl. Acad. Sci. USA **114**, 6996 (2017).
[22] Y. A. Gerasimenko, I. Vaskivskyi, M. Litskevich, J. Ravnik, J. Vodeb, M. Diego, V. Kabanov, and D. Mihailovic, Nat. Mater. **18**, 1078 (2019).
[23] X. L. Wu and C. M. Lieber, Phys. Rev. Lett. **64**, 1150 (1990).
[24] I. Lutsyk, M. Rogala, P. Dabrowski, P. Krukowski, P. J. Kowalczyk, A. Busiakiewicz, D. A. Kowalczyk, E. Lacinska, J. Binder, N. Olszowska, M. Kopciuszynski, K. Szalowski, M. Gmitra, R. Stepniewski, M. Jalochowski, J. J. Kolodziej, A. Wysmolek, and Z. Klusek, Phys. Rev. B **98**, 195425 (2018).
[25] See Supplemental Material at http://link.aps.org/supplemental/10.1103/PhysRevMaterials.4.064007 for more details on the line-cut profiles in the FT of STM topography, STM topography on pristine 1T-TaS_2 for calculating the polaronic pair distribution functions, stability of the disordered charge order, and comparison with the amorphous state induced by ultrafast laser.
[26] J. Vodeb, V. V. Kabanov, Y. A. Gerasimenko, R. Venturini, J. Ravnik, M. A. van Midden, E. Zupanic, P. Sutar, and D. Mihailovic, New J. Phys. **21**, 083001 (2019).
[27] J. Vodeb, V. V. Kabanov, Y. A. Gerasimenko, I. Vaskivskyi, J. Ravnik, and D. Mihailovic, J. Supercond. Nov. Magn. **32**, 3057 (2019).
[28] G. Baskaran, Physica C: Supercond. **417**, 150 (2005).
[29] S. Qiao, X. Li, N. Wang, W. Ruan, C. Ye, P. Cai, Z. Hao, H. Yao, X. Chen, J. Wu, Y. Wang, and Z. Liu, Phys. Rev. X **7**, 041054 (2017).
[30] K. Bu, W. Zhang, Y. Fei, Z. Wu, Y. Zheng, J. Gao, X. Luo, Y.-P. Sun, and Y. Yin, Commun. Phys. **2**, 146 (2019).
[31] E. G. C. P. van Loon, M. Schüler, D. Springer, G. Sangiovanni, J. M. Tomczak, and T. O. Wehling, arXiv:2001.01735.